A Nine-layer Atmospheric General Circulation Model and Its Performance

Wu Guoxiong (吴国雄), *Liu Hui* (刘 辉), *Zhao Yucheng* (赵宇澄), and *Li Weiping* (李伟平),
Lab. of Atmospheric Sciences and Geophysical Fluid Dynamics (LASG),
Institute of Atmospheric Physics, Chinese Academy of Sciences, Beijing, 100080
Received May 22, 1995

ABSTRACT

Different versions of a new nine-layer general circulation model which is rhomboidally truncated at zonal wave number 15 (L9R15) are introduced in this paper. On using the observed global monthly sea surface temperature (SST) and sea ice (SI) data from 1979 to 1988 offered by the international Atmospheric Model Inter-comparison Program (AMIP), these different model versions were integrated for the ten-year AMIP period. Results show that the model is capable of simulating the basic states of the atmosphere and its interannual variability, and in performing reasonable sensitivity experiments.

Key words: General circulation model, Numerical simulation, Interannual variability, Sensitivity experiment

I. INTRODUCTION

Since the early days of LASG, great efforts have been contributed to the development of general circulation models (GCM) and to the simulation of the climate system and its variability. Our first GCM was constructed by Zeng and his cooperators (1987 and 1989). Despite its low vertical resolution, this model was successful in modelling climate characteristics (Liang, 1986; Xue, 1992), in producing sensitivity experiments (Zhang et al., 1989), in coupling with other climate sub-systems (Zhang, 1992), and in predicting short-term climate variations (Zeng, 1990; Yuan, 1990). Besides, due to its economy in calculation and concise physics, it has become an ideal educational model. Based upon this model, many talented young scientists have grown up, and many valuable experiences have been accumulated.

One of the main targets of LASG is to construct a climate system model. To this regard, vertical resolution is crucial for treating the interactions at boundaries between the atmosphere and the other climate sub-systems. Since the end of 1991, we have introduced a nine-layer spectral model which is rhomboidally truncated at zonal wave number 15, and engaged in a series of work for its reformation and development. The model was originally transferred by Lin (1991) from the version of Simmonds (1985). It suffered from serious global cooling and, particularly, from false "negative orography" effects due to the low truncation in the spectral expansion of orography. Around steep mountains, such as the Tibetan plateau, Rockies, Andes, and Antarctica, many false systems and systematic errors were found. Our efforts during the last years mainly include the introduction of more realistic external forcing to the model atmosphere, and the reformation of its dynamic framework by subtracting "a standard atmosphere" from the set of governing equation (Zeng, et al., 1963; Phillips, 1973). These make the model perform much better. In this paper, we show how the experiences accumulated at LASG were used to reform this L9R15 model, and how it behaves in modelling the climate mean states and their variability. Some applications of the model to sensitivity experiments are also reported.

II. DYNAMICAL FRAMEWORK

1. *Model Version Set–1: The Governing Equations*

With spherical coordinates in horizontal and σ–coordinates in the vertical, the system which governs the atmospheric motions can be expressed in terms of the prognostic equations for the vertical component of relative vorticity,

$$\frac{\partial \zeta}{\partial t} = -\frac{1}{a\ \cos^2\varphi}\left[\frac{\partial A}{\partial \lambda} + \cos\varphi \frac{\partial B}{\partial \varphi}\right] - 2\Omega\left(D\sin\varphi + \frac{V}{a}\right)$$

$$+ \vec{k} \cdot \nabla \times (\vec{F}_h + \vec{F}_V), \tag{1}$$

the horizontal divergence,

$$\frac{\partial D}{\partial t} = -\frac{1}{a\ \cos^2\varphi}\left[\frac{\partial B}{\partial \lambda} - \cos\varphi \frac{\partial A}{\partial \varphi}\right] + 2\Omega\left(\zeta\sin\varphi - \frac{U}{a}\right)$$

$$- \nabla^2(E + \Phi' + RT_0 q) + \nabla \cdot (\vec{F}_h + \vec{F}_V), \tag{2}$$

the continuity of mass,

$$\frac{\partial q}{\partial t} = -\vec{V} \cdot \nabla q - D - \frac{\partial \dot{\sigma}}{\partial \sigma}, \tag{3}$$

the diagnostic hydrostatic equation,

$$\frac{\partial \Phi}{\partial \sigma} = -\frac{RT}{\sigma}, \tag{4}$$

the prognostic equation of thermodynamics,

$$\frac{\partial T}{\partial t} = -\frac{1}{a\ \cos^2\varphi}\left[\frac{\partial}{\partial \lambda}(UT'') + \cos\varphi \frac{\partial}{\partial \varphi}(VT'')\right] +$$

$$T''D + \Gamma\dot{\sigma} + \frac{RT}{C_p}[\tilde{D} + (\vec{V} + \tilde{\vec{V}}) \cdot \nabla q] + H + F_h^T + F_V^T, \tag{5}$$

and the prognostic equation for moisture,

$$\frac{\partial M}{\partial t} = -\frac{1}{a\ \cos^2\varphi}\left[\frac{\partial}{\partial \lambda}(UM'') + \cos\varphi \frac{\partial}{\partial \varphi}(VM'')\right] +$$

$$M''D - \dot{\sigma}\frac{\partial M}{\partial \sigma} + C + F_h^M + F_V^M. \tag{6}$$

Here, $U = u\cos\varphi$, $V = v\cos\varphi$, and

$$A = \zeta U + \dot{\sigma}\frac{\partial V}{\partial \sigma} + \frac{RT''}{a}\cos\varphi\frac{\partial q}{\partial \varphi}, \tag{7}$$

$$B = \zeta V - \dot{\sigma}\frac{\partial U}{\partial \sigma} - \frac{RT''}{a}\frac{\partial q}{\partial \lambda}, \tag{8}$$

$$E = \frac{U^2 + V^2}{2\cos^2\varphi}, \tag{9}$$

$$\tilde{A} = \int_1^0 A d\sigma, \tag{10}$$

$$\tilde{A}^{\sigma} = \int_1^{\sigma} A d\sigma, \tag{11}$$

$$q = \ln p_* \ , \tag{12}$$

and

$$\Gamma = \frac{RT}{C_p \sigma} - \frac{\partial T}{\partial \sigma} \ , \tag{13}$$

is the static stability. The subscript [0] denotes a horizontal mean value averaged over a σ–surface, and the superscript [″] denotes the deviation from that mean, i.e.,

$$T(x,y,\sigma;t) = T_0(\sigma;t) + T''(x,y,\sigma;t), \tag{14}$$

$$\Phi(x,y,\sigma;t) = \Phi_0(\sigma;t) + \Phi''(x,y,\sigma;t). \tag{15}$$

The other symbols are conventional.

2. *Standard Atmosphere Subtraction (SAS)*

One of the major problems in employing σ–coordinate is associated with the calculation of pressure gradient force, which becomes a small difference between two large terms, i.e.,

$$-\nabla_p \Phi = -\nabla_\sigma \Phi - RT\nabla_\sigma q.$$

If we introduce a standard atmosphere in which Φ and T are functions of p only, and let an overbar denote variables of the standard atmosphere, then we have the exact balance between these two large terms for the standard atmosphere, i.e.,

$$-\nabla_p \overline{\Phi} = -\nabla_\sigma \overline{\Phi} - R\overline{T}\nabla_\sigma q \equiv 0. \tag{16}$$

Let a superscript [′] denote the deviation from this standard atmosphere, i.e.,

$$\begin{cases} \Phi(x, y, p;\ t) = \overline{\Phi}(p) + \Phi'(x, y, p;\ t), \\ T(x, y, p;\ t) = \overline{T}(p) + T'(x, y, p;\ t) \end{cases} \tag{17}$$

Now, the pressure gradient force

$$-\nabla_p \Phi = -\nabla_\sigma \Phi' - RT'\nabla_\sigma q$$

becomes the difference between two small terms due to the subtraction of the standard atmosphere. Higher accuracy is then achieved. Since in such a standard atmosphere, $\overline{T}$ and $\overline{\Phi}$ are independent of time, the prognostic equation for temperature and the hydrodynamic equation have to be modified, and a set of equations for the deviation atmosphere has to be established (Phillips, 1973; Zeng, 1963).

3. *Model Version Set–2: Standard Atmosphere with Constant Lapse Rate*

A simple way to introduce SAS into a GCM is by taking a constant temperature lapse rate. This was firstly done by Zeng and his cooperators (1987) for the 2–layer grid point AGCM / IAP, and proved to give remarkable improvement to the model behaviour. It was later employed by Chen and Simmons (1989) to a spectral model with triangular truncation. Here, we will briefly describe how this idea is employed in our 9–layer model by following the same procedure. Since the lapse rate is constant, the internal gravity wave speed C_0 will be constant. We then have,

$$C_0^2 = \frac{R\overline{T}^2}{g}\left(\frac{g}{C_p} + \frac{d\overline{T}}{dz}\right) = \frac{R\overline{T}^2}{g}(\gamma_d - \gamma) = \text{constant}, \tag{19}$$

$$\frac{\partial \overline{\Phi}}{\partial \ln p} = -\mathrm{R}\overline{\mathrm{T}}. \tag{20}$$

From these, the following analytical solutions can be obtained:

$$\overline{T}(p) = \frac{Y}{R} + \frac{X}{C_p}\left(\frac{p}{p_{00}}\right)^{R/C_p} \equiv \overline{T}_2 + \overline{T}_1\left(\frac{p}{p_{00}}\right)^{R/C_p}, \tag{21}$$

$$\overline{\Phi}(p) = X\left[1 - \left(\frac{p}{p_{00}}\right)^{R/C_p}\right] - Y\ln\left(\frac{p}{p_{00}}\right), \tag{22}$$

where,

$$X \equiv C_p\left(\overline{T}_{00} - \frac{C_p}{R^2}C_0^2\right), \tag{23}$$

$$Y \equiv \frac{C_p}{R}C_0^2. \tag{24}$$

Let $T_{00} = 288\mathrm{K}$, $p_{00} = 1013\mathrm{hPa}$, the analytical solutions for surface pressure and temperature can then be obtained:

$$\ln(\overline{p}_*) = \ln p_{00} + \frac{C_p}{R}\ln\left[1 - \frac{1}{X}(\Phi_* - Y\ln p_{00} + Y\ln\overline{P}_*)\right], \tag{25}$$

$$\overline{T}_* = \overline{T}(\ln\overline{p}_*) = Y_0 + X_0\exp(\frac{R}{C_p}\ln\overline{p}_*) = Y_0 + \frac{X}{C_p}(\overline{p}_* / p_{00})^{R/C_p}, \tag{26}$$

where, $Y_0 = Y/R$, $X_0 = (\overline{T}_{00} - Y_0)/p_{00}^{R/C_p}$. By defining the deviation variables

$$T'(x,y,\sigma;t) = T_a(\sigma;t) + T''(x,y,\sigma;t), \tag{27}$$

$$\Phi'(x,y,\sigma;t) = \Phi'_* + \Phi''(x,y,\sigma;t), \tag{28}$$

and using the relation

$$\Phi'_* = \Phi'(q_*) = R\overline{T}_S(q_* - \overline{q}_*) + R\overline{T}'_*(q_* - \overline{q}_*), \tag{29}$$

where,

$$\overline{T}_S = 288\text{K}, \quad \overline{T}'_* = \overline{T}_* - \overline{T}_S, \tag{30}$$

then carrying some manipulations, the following equation set for the deviation atmosphere can be obtained:

$$\frac{\partial\zeta}{\partial t} = -\frac{1}{a\cos^2\varphi}\left[\frac{\partial A}{\partial\lambda} + \cos\varphi\frac{\partial B}{\partial\varphi}\right] - 2\Omega\left(D\sin\varphi + \frac{V}{a}\right) + \vec{k}\cdot\nabla\times(\vec{F}_h + \vec{F}_V), \tag{31}$$

$$\frac{\partial D}{\partial t} = \frac{1}{a\cos^2\varphi}\left[\frac{\partial B}{\partial\lambda} - \cos\varphi\frac{\partial A}{\partial\varphi}\right] + 2\Omega\left(\zeta\sin\varphi - \frac{U}{a}\right) - \nabla^2(E + \Phi'' + R(T_a + \overline{T}_S)q_* - R\overline{T}_S\overline{q}_*) - \nabla^2(R\overline{T}'_*(q_* - \overline{q}_*)) + \vec{k}\cdot(\vec{F}_h + \vec{F}_V), \tag{32}$$

$$\frac{\partial T'}{\partial t} = (\frac{Y}{C_p\sigma} + \Gamma_a)(\tilde{D} - \tilde{D}^\sigma) + \sigma\frac{\partial T_a}{\partial\sigma}\tilde{D} + Z, \tag{33}$$

$$\frac{\partial M}{\partial t} = -\frac{1}{a\cos^2\varphi}\left[\frac{\partial}{\partial\lambda}(UM'') + \cos\varphi\frac{\partial}{\partial\varphi}(VM'')\right] + M''D - \sigma\frac{\partial M}{\partial\sigma} + S, \tag{34}$$

$$\frac{\partial q_*}{\partial t} = -\vec{V}\cdot\nabla q - D - \frac{\partial\dot{\sigma}}{\partial\sigma}, \tag{35}$$

$$\frac{\partial\Phi'}{\partial\ln\sigma} = -RT', \tag{36}$$

where

$$Z = -\nabla\cdot\vec{V}T' + T'D + \Gamma''(\tilde{D} - \tilde{D}^\sigma) + \sigma\frac{\partial T''}{\partial\sigma}\tilde{D} +$$

$$\nabla q \cdot \left\{ \left(\frac{Y}{C_p \sigma} + \Gamma' \right) (\vec{\tilde{V}} - \vec{\bar{V}}) + \sigma \frac{\partial T'}{\partial \sigma} \vec{\tilde{V}} + \frac{R(\bar{T}_2 + T')}{C_p} \vec{V} \right\} , \tag{37}$$

$$M'' = M - M_a . \tag{38}$$

In our study, equations (1) to (6) were defined as Set−1, and equations (31) to (36) were defined as Set−2. They were used to construct respectively version 1, and version 2 of the L9R15 AGCM.

The model atmosphere is divided into 9 vertical layers as shown in Fig. 1, and rhomboidally truncated at wave number 15 in the horizontal, as described by Manabe et al. (1975). With the same physical processes which are to be described in the following section, the two versions were integrated for the AMIP period ranging from Jan. 1, 1979 to Dec. 31, 1988. SST and SI were prescribed from the AMIP data set. After making the 10−year means, we present the January mean distributions of the 500 hPa geopotential height for version 1 and version 2 respectively in Fig. 2. In version 1, many unrealistic perturbations were found around large and high mountains, such as the Greenland Highland, the Rockies, Tibetan Plateau, Andes, and the Antarctic Highlands (Fig. 2a). After the scheme SAS was introduced to give version 2, these unrealistic perturbations were removed, and the model results (Fig. 2b) become much closer to observations.

4. *Model Version Set−3: Variable Lapse Rate*

In the real atmosphere, both the lapse rate and the speed of gravity waves change with height. To better present the standard atmosphere, in (19) we let C_0^2 be a function of p rather than constant. This is equivalent to setting

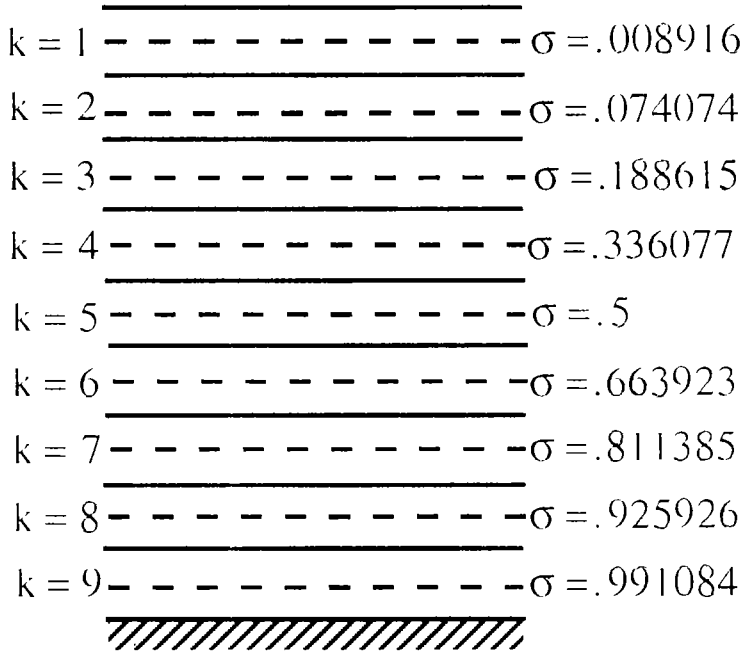

Fig. 1. Vertical distribution of the nine layers of the L9R15 model.

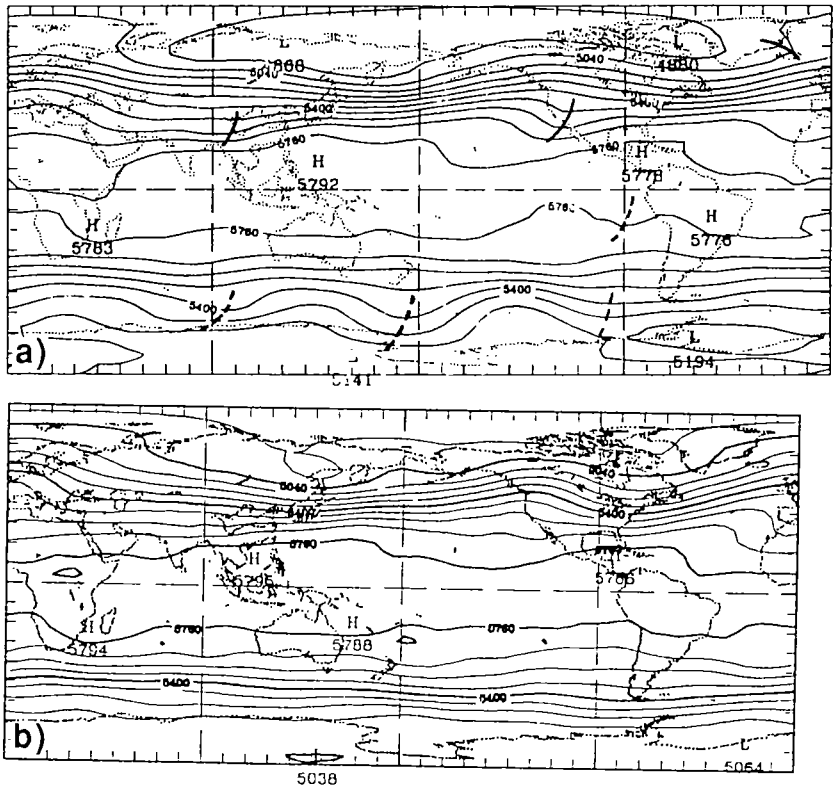

Fig. 2. The January mean 500 hPa geopotential height simulated respectively by version 1 of the model (a), and by version 2 in which SAS scheme has been employed (b). Units are in 10 gpm.

$$\frac{\partial \overline{T}}{\partial p} = \Gamma(p).$$

Once $\Gamma(p)$ is known, then together with (20), $\overline{T}(p)$ and $\overline{\Phi}(p)$ can be determined. In our model version 3, $\overline{T}(p)$ and $\overline{\Phi}(p)$ are calculated based upon the 5–year mean ECMWF data compiled by Wu and Liu (1987); the results are listed in Table 1.

Table 1. The ECMWF Standard Atmosphere Based upon the Annual Mean Data Averaged from Sep. 1979 to Aug. 1984 as Compiled by Wu and Liu (1987)

Pressure (hPa)	Temperature (°C)	Height (gpm)
30	−54.6	23000
50	−59.4	20000
70	−62.0	18000
100	−63.0	16210
150	−59.9	13620
200	−54.4	11790
250	−48.9	10360
300	−42.5	9160
400	−29.1	7180
500	−18.1	5570
700	−2.67	3010
850	5.23	1460
1000	11.1	110

To obtain the thermodynamic equation for the deviation atmosphere for version 3, we let

$$\overline{T}(p) = \overline{T}_2(p) + \frac{\partial \overline{T}}{\partial p}\frac{C_p}{R}p, \tag{39}$$

$$T'(x,y,\sigma;t) = T_a(\sigma;t) + T''(x,y,\sigma;t) \tag{40}$$

for the standard and deviation atmosphere respectively, and set

$$\overline{T}_2 = \overline{T}_{2a}(\sigma;t) + T'_2(x,y,\sigma;t). \tag{41}$$

Following the same procedure, we can then arrive at a new thermodynamic equation for version 3, which is in parallel to (33) of version 2:

$$\frac{\partial T'}{\partial t} = (\frac{R\overline{T}_{2a}}{C_p\sigma} + \Gamma_a)(\tilde{D} - \tilde{D}^\sigma) + \sigma\frac{\partial T_a}{\partial \sigma}\tilde{D} + ZZ, \tag{42}$$

in which,

$$ZZ = -\nabla \cdot \vec{V}T' + T'D + (\frac{RT'_2}{C_p\sigma} + \Gamma'')(\tilde{D} - \tilde{D}^\sigma) + \sigma\frac{\partial T''}{\partial \sigma}\tilde{D} +$$

$$\nabla q \cdot \left\{(\frac{R\overline{T}_2}{C_p\sigma} + \Gamma')(\tilde{\vec{V}} - \tilde{\vec{V}}) + \sigma\frac{\partial T'}{\partial \sigma}\tilde{\vec{V}} + \frac{R(\overline{T}_2 + T')}{C_p}\vec{V}\right\}. \tag{43}$$

The other governing equations in version 3 are the same as those in version 2. This version has also been integrated for the same AMIP period together with an updated albedo scheme which is to be described in the following subsection. Results from this version will be presented in Sections 3 and 4.

III. PHYSICAL PROCESSES

The physical processes included in the model have been described in detail in the Technical Report No. 3 of LASG (Liu, et al., 1995; also referred to Lin, 1991). Here only a brief introduction is given.

1. *Radiation Scheme*

The radiation heating for the model is computed using the scheme of Manabe and Strickler (1964) and Manabe and Wetherald (1967). The radiation absorbers include cloud, water vapour, CO_2 and O_3. The mixing ratio of CO_2 is assumed to be a constant 4.56×10^{-4} throughout the atmosphere. Zonally averaged seasonal mean values of ozone distribution were taken from Dopplick (1974). The high–, middle–, and low–level clouds are considered but not as prognostic variables. Cloud amounts and heights are prescribed in terms of the climatology of the observed values of London (1957), which are zonally mean and seasonally averaged. The diurnal variation of solar insolation has been eliminated by use of an effective mean zenith angle and daylight duration for each latitude (Manabe et al., 1961) and the radiation scheme is calculated every 24 hours.

In model version 2, the albedo of land and sea varies only latitudinally and is derived from the charts of Posey and Clapp (1964). Over sea ice the albedo is fixed at 0.65 and 0.7 for the Northern and Southern Hemisphere, respectively. Over snow the albedo is 0.65 and 0.85 for the two hemispheres, respectively. In version 3, monthly averaged and localized albedo data generated from satellite remote sensing at the Canadian (Li, Z. Q., 1994, personal communication) were employed. This gives remarkable improvement for rainfall simulation over

continental areas, particularly over the North Africa.

2. *Convection and Condensation*

The model's convection and condensation are parameterized using the dry moist convective adjustment scheme (Manabe et al., 1965) independent of cloud.

3. *Boundary Layer*

The stress and the sensible and latent heat fluxes at the surface are given by the bulk aerodynamic parameterization:

$$\bar{\tau}_* = \rho_1 C_d |\vec{v}_1| \vec{v}_1, \tag{44}$$

$$H_* = \rho_1 \delta c_p \frac{C_d}{D} |\vec{v}_1| (\theta_* - \theta_1), \tag{45}$$

$$E_* = L\rho_1 c_W \frac{C_d}{D} |\vec{v}_1| (M_* - M_1) \tag{46}$$

with $\delta = (p / p_0)^{R/c_p}$, the subscripts asterisk and "1" denote the surface and the lowest model level, respectively. D is a constant taken to be 0.74. The drag coefficient C_d is obtained from the Monin–Obukov formula and is dependent on hydrostatic stability. The gustiness parameter is set to 1.0 m / s. The wetness parameter C_W assumes values of 0.25 and 1.0 over land and sea, respectively. It is assumed that there is no heat conduction into the soil so that the equation of heat balance becomes

$$S\downarrow + L\downarrow = \sigma_S T_*^4 + H_* + E_* + Q_i, \tag{47}$$

where $S\downarrow$ and $L\downarrow$ are the net downward insolation and net downward long wave radiation at the surface. Q_i is added only over sea ice and represents heat conduction through a constant ice thickness of 2 m with sub–ice sea water temperature fixed at 271.2K. The equation is solved using an iteration method and once T_* is known the fluxes of sensible and latent heat can be determined.

The daily SST and SI are interpolated from the AMIP monthly mean data. The snow cover over land is prescribed according to observed monthly climatology. Runoff into ocean is not included in the current model.

4. *Horizontal and Vertical Diffusion*

In the prognostic equations the sub–truncation scale processes are parameterized as follows:

$$\vec{k} \cdot \nabla \times \vec{F}_h = K_H (\nabla^2 \zeta + \frac{2\zeta}{a^2}), \tag{48}$$

$$\nabla \cdot \vec{F}_h = K_H (\nabla^2 D + \frac{2D}{a^2}), \tag{49}$$

$$F_h^T = K_H \nabla^2 T, \tag{50}$$

$$F_h^M = K_H \nabla^2 M, \tag{51}$$

$$(\vec{F}_V, F_V^T, F_V^M) = \frac{g}{p_*} \frac{\partial}{\partial \sigma} \{\vec{\tau}, H / c_p, E\}, \tag{52}$$

where

$$\vec{\tau} = \rho^2 \frac{g}{p_*} K_V \frac{\partial \vec{V}}{\partial \sigma}, \tag{53}$$

$$\frac{H}{c_p} = \delta \rho^2 \frac{g}{p_*} K_V \frac{\partial \theta}{\partial \sigma}, \tag{54}$$

$$E = \rho^2 \frac{g}{p_*} K_V \frac{\partial M}{\partial \sigma}, \tag{55}$$

where, K_H is taken to be $2.5 \times 10^5 \mathrm{m^2 s^{-1}}$, but is applied only to the high wave number portion of the spectrum in the lower seven model levels, while it is applied over the entire spectrum in the uppermost two model layers. Here, K_V defines the vertical diffusion coefficient which is given in terms of a mixing length and the magnitude of wind shear:

$$K_V = \rho \frac{g}{p_*} \mu^2 \left| \frac{\partial \vec{V}}{\partial \sigma} \right| . \tag{56}$$

In the present case, μ is assumed to be 30 m for $\sigma \geqslant 0.5$ and 0 for $\sigma < 0.5$.

IV. SIMULATION OF THE MEAN CLIMATE

In this section we present the performance of the model in simulating the climate. Fig. 3 shows the inter comparison of sea level pressure (SLP) between the time–mean observations (b and d), and simulations (a and c) for January and July, respectively. The Aleutian low and Icelandic low, and Eurasian high and North American high in the boreal winter, the continental low and oceanic high in the boreal summer, and the permanent oceanic high and the pronounced "roaring forties" in the Southern Hemisphere are all simulated remarkably well. The simulated surface temperature (figures not shown) is also in very good correspondence with observations. In Fig. 4 is shown the precipitation, with the same layout as in Fig. 3, for Dec., Jan., and Feb. (DJF), and for Jun., Jul., and Aug. (JJA), respectively. During DJF (Fig. 4a), the dryness over the boreal continent, the ITCZs, and the heavy precipitation centres over the southern America and the southeast of Africa are reproduced. During JJA (Fig. 4c), the observed three centres of tropical rainfall are also represented in the model. The precipitation along the monsoon trough is particularly well reproduced both in location and in intensity. Fig. 5 shows the distributions of the averaged wind field at 1000 hPa. The strong trade winds in the tropics, the "roaring forties" in the Southern Hemisphere, and the predominance of the mid–latitude westerlies are all reproduced reasonably. In the equatorial Indian Ocean and South China Sea region, strong northeasterly winter monsoon and southwestly summer monsoon are also simulated successfully.

The simulated mean circulations in the upper troposphere are also in good agreement with the corresponding observations (see Liu et al., 1995), but systematic errors exist. The main error shows up in the upper layer geopotential heights, which are lower than observations (e.g., see Fig. 2). This is mainly due to the fact that the modelled troposphere is colder than reality by about 1°C in most latitude zones (Liu, et al., 1995).

V. SIMULATION OF SEASONAL CHANGE

The model has been employed to simulate seasonal changes. As one example, we have examined the impacts on monsoon onset of the spring snow melt over the Tibetan Plateau. We chose this issue because many studies (e.g., Ji, 1975; Chen, 1981) have shown that when there is more snow accumulation in the spring period over the Tibetan plateau, the onset of

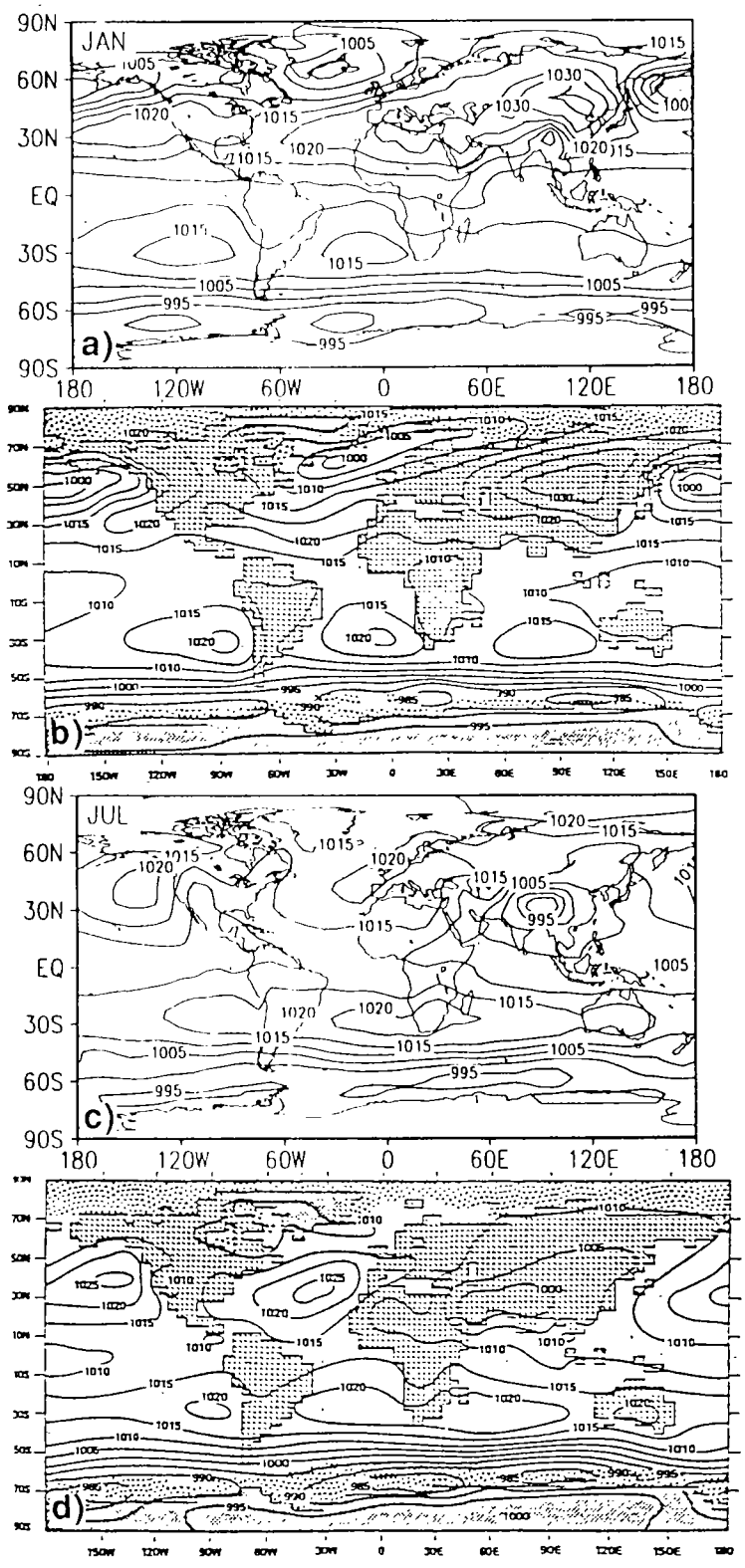

Fig. 3. Distribution of monthly mean sea-level pressure for January and for July in the L9R15 AGCM simulation for the period 1979–1988 (a and c), and in observation (b and d) from Schlesinger and Gates (1980), respectively. Interval in 5 hPa.

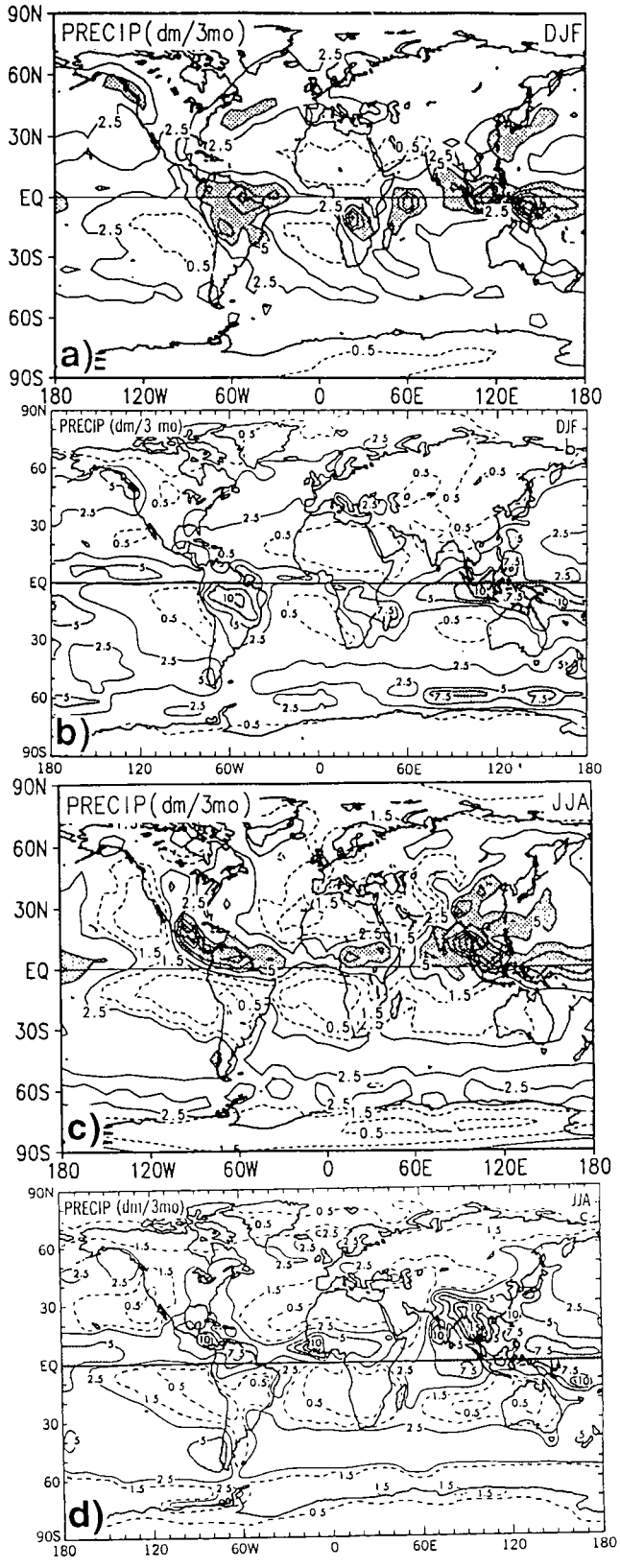

Fig. 4. Distribution of seasonal mean precipitation for DJF and for JJA in the L9R15 AGCM simulation for the period 1979–1988 (a and c), and in observation (b and d) from Peixoto and Oort (1992). Unit in dm / (3 months)

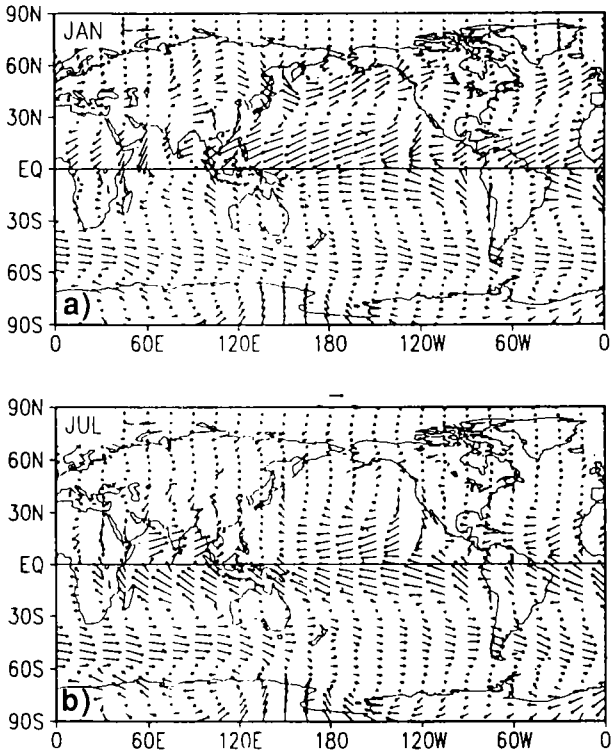

6.2

Fig. 5. Distribution of the monthly mean wind field at 1000 hPa for January (a) and for July (b) produced in the L9R15 AGCM simulation for the period 1979–1988.

the Indian monsoon is delayed, and vice versa.

We first fixed the solar angle, length of day, SI and SST at their climate mean January 1 values, and integrated the model for half a year to reach a quasi–steady state. This state was then selected as the common initial condition for January 1 in different experiments. Three experiments were designed: the control experiment (CON) uses all the climate mean data as external forcing. The other two experiments MSN and LSN were constructed to represent more, and less spring snow cover over the Plateau. All these experiments allow for annual cycles, and were integrated from the common initial values at January 1 to October 31. In each experiment, the daily values of SI and SST were prescribed according to their climate values which were averaged over the AMIP period.

The only difference arises through the different treatment of the snow cover over the plateau. In Fig. 6 are shown the distributions of climate mean snow cover used in the model for Jan., Feb., and Mar., respectively. There is no snow cover in April over the central and eastern parts of the plateau. These are used as given for the CON case. In the MSN case, the distributions of snow cover for the model months of Feb. to April were replaced by those of the preceding month's climate. In the LSN case, the distributions of snow cover over the plateau for the model months of Jan. to Mar. were replaced by those of the following–month's climate. Based upon the experiment outputs, in Fig. 7 are shown the total downward radiation flux reaching the ground surface (a) and the surface upward sensible heat flux (b), both averaged over the four grid points which represent the central and eastern parts of the plateau. As

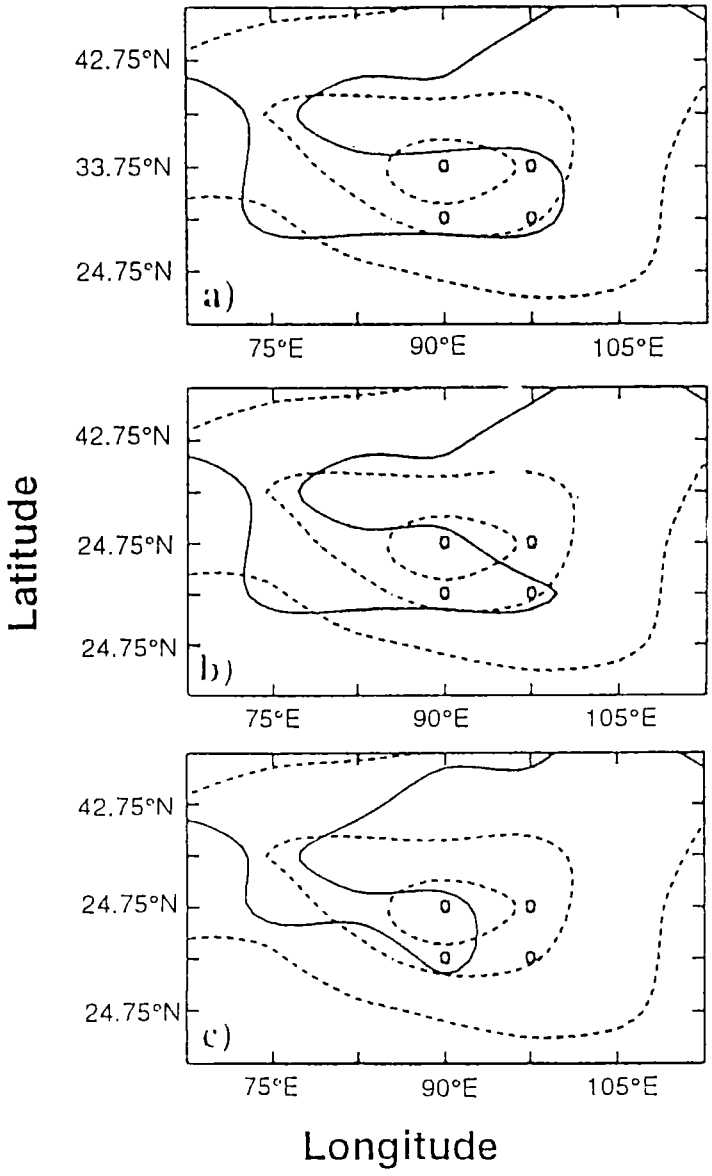

Fig. 6. Distribution of snow cover over the Tibetan Plateau as was used in the control experiment CON. The dashed curves denote the region where the surface pressure is less than 600, 700, and 900 hPa, respectively. The blank circles indicate the locations of the four grid points to be used in the following calculations. (a) January; (b) February; (c) March.

expected, both the radiation income at the surface and the surface sensible heating to the atmosphere increase in the LSN case, but decrease in the MSN case. The change of the downward radiation flux is as high as 50 WM^{-2}. Another prominent feature demonstrated by Fig. 7 is that the plateau is a sensible heat sink in winter and heat source in summer. This agrees well with the calculations of Ye et al. (1979) based on observation data estimates. From this point of veiw, more snow cover delays the spring heating of the plateau to the atmosphere. This then will affect the seasonal change at least in the region. Fig. 8 shows the evolution of the westerlies at 950 hPa along the 13.5°N latitude. It shows that in the model atmosphere over

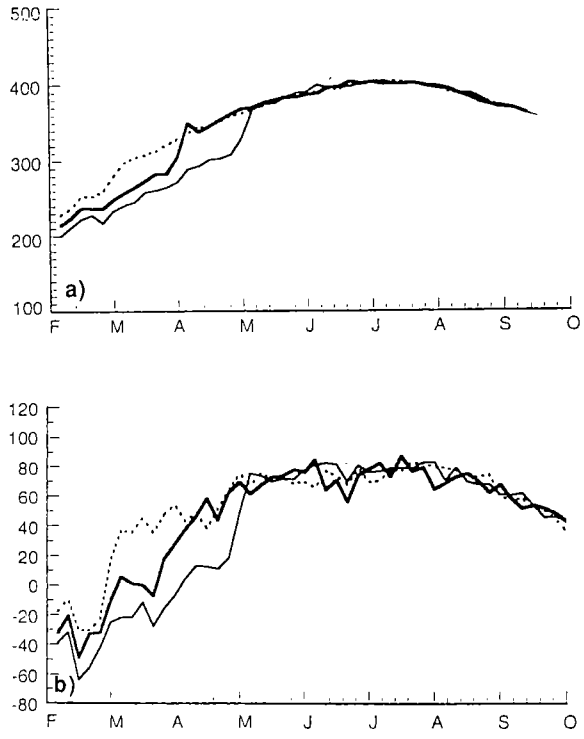

Fig. 7. Time evolutions of the downward radiation flux at the ground surface (a), and the upward sensible heat flux (b) averaged over the four grid points as shown in Fig. 6. Units in WM^{-2}. Heavy solid, light solid, and dotted curves represent the results from the CON, MSN, and LSN experiments, respectively.

the Bay of Bengal, the westerlies associated with southwesterly monsoon is establlished in the late May (Fig. 8a), in good agreement with reality (Tao and Chen, 1988). In MSN case, the monsoon onset is delayed by two to three weeks. Fig. 8b shows that strong anomalous westerlies in the region are established around June 17. These results are in good agreement with observational data analyses reported by Chen (1981).

VI. SIMULATION OF INTERANNUAL VARIABILITY

During the AMIP period, there were two El Niño events (1982–1983, 1986–1987), and two La Nina events (1984 and 1988). In Fig. 9 are shown the simulated evolutions of the equatorial anomalous SLP and anomalous wind fields, respectively. In the eastern equatorial Pacific region, the anomalous SLP was negative during the warm events and positive during the cold events. Anomalous winds are from positive to negative anomalous SLP. Eastward propagation of the SLP and wind anomalies are prominent, particularly in the 1982–1983 case. These are in good agreement with the diagnoses of Wang (1995) based on observational data.

VII. SUMMARY

In this paper, we described how the SAS scheme was extended to our L9R15 model, and demonstrated that the use of this scheme has improved the model behaviour remarkably. It was shown that the model is capable in simulating the climate mean states, such as sea level

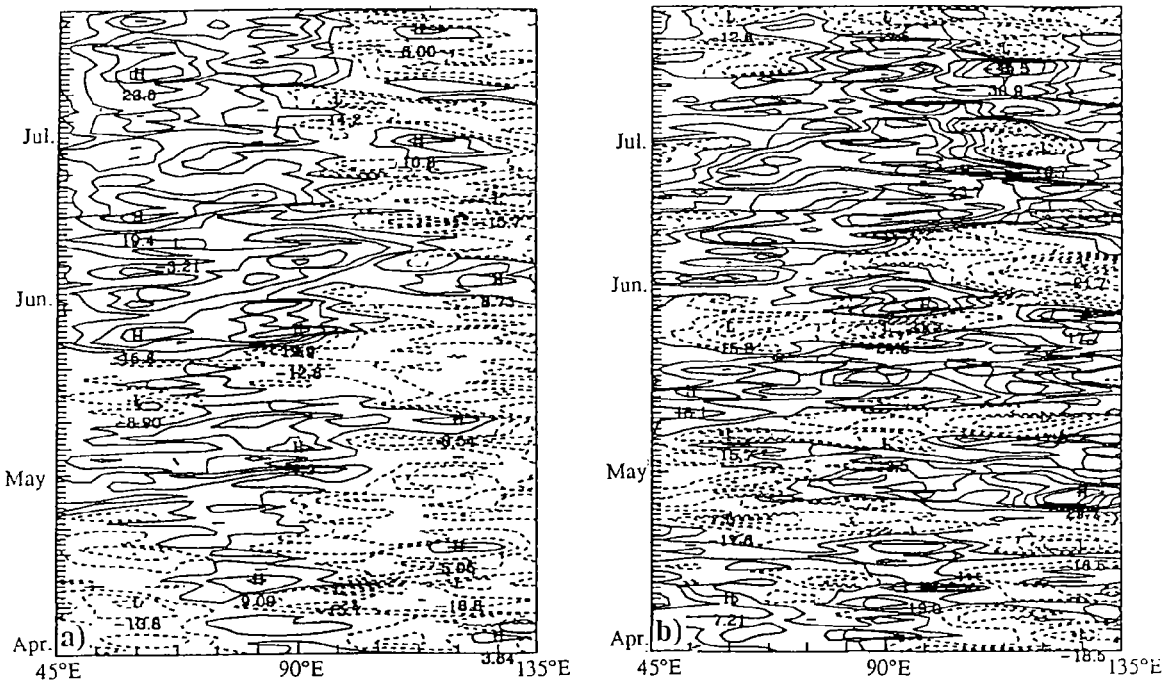

Fig. 8. Time–longitude plot of the u–component at 950 hPa along the 13.5°N latitude circle. Interval in 4 ms^{-1}. Dashed curve indicates negative value. (a) In the CON experiment; (b) in the MSN–CON case.

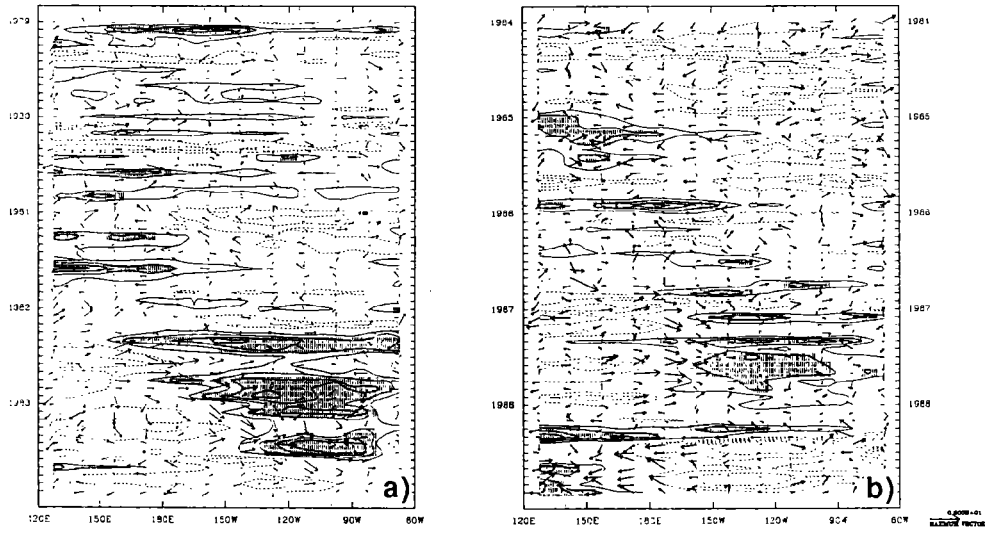

Fig. 9. Time–longitude plots of the anomalous sea level pressure in contours and surface wind in vectors. Solid and dashed contours denote negative and positive values, respectively. Interval in 0.5 hPa, and shading indicates the negative SLP anomaly is stronger than 1.0 hPa.

pressure, precipitation, and wind fields. It is also successful in simulating monsoon onset and some interannual variability. However, systematic errors also exist in our model as in other GCMs. Considerable efforts have been contributed to the improvement of its physical processes, particularly the land surface processes and radiation processes. Recently, this model has been successfully coupled with a 20– layer ocean general circulation model which was designed by Zhang and his cooperators (Zhang et al., 1994), and produced good simulations (Liu et al., 1995). We hope that through continuous efforts, we would be able to further improve the model's behaviour and to simulate the climate system more accurately.

The authors would like to thank Professor Lin Yuanbie for his kind help in the transfer of his original model version, and in the valuable discussions during our model reformation and development.

REFERENCES

Chen, J. B. and A. J. Simmons (1989), Sensitivity of medium–range weather forecasts to the use of reference atmosphere, *Adv. Atmos. Sci.*, **7:** 275–293.

Chen, L. T. and Z. X. Yan (1981), Statistics of the impacts on early summer monsoon of the anomalous snow cover in winter and spring over the Tibetan Plateau, *Proceedings of the Symposium of the Tibetan Plateau Meteorology*, Science Press, 151–161.

Dopplick, T. G. (1974), Radiative heating in the atmosphere, The general circulation of the tropical atmosphere and interactions with extratropical latitudes, Vol. 2, MIT Press.

Ji, J. J., K. R. Li and W. Y. Sa (1975), Tibetan Plateau snow accumulation, *Meteorology*, **12:** 8–10 (in Chinese).

Liang, X. Z. (1986), *Design of the IAP AGCM and numerical climate simulation*, Ph.D. Theses, Inst. Atmos. Phy., Chinese Academy of Sciences, 250 pp.

Lin, Yuanbie (1991), *General circulation experiments at Guangzhou Institute of Tropical Oceanography and Meteorology*, 14 pp.

Liu Hui and Wu Guoxiong et al. (1995), Description for a 9–Layer Spectral Climate Model (L9R15), LASG Technical report No. 3.

London, J. (1957), A study of the atmospheric heat balance, Rep., Dept. Meteor. Oceanogr., New York University, 99 pp.

Manabe, S. and F. Moller (1961), On the radiation equilibrium and heat balance of the atmosphere, *Mon. Wea. Rev.*, **89:** 503–532.

Manabe, S., J. Smagorinsky and R. F. Strickler (1965), Simulated climatology of a general circulation model with a hydrological cycle, *Mon. Wea. Rev.*, **93:** 769– 798.

Manabe, S. and R. F. Strickler (1964), Thermal equilibrium of the atmosphere with a convective adjustment, *J. Atmos. Sci.*, **21:** 361–385.

Manabe, S. and R.T. Wetherald (1967), Thermal equilibrium of the atmosphere with a given distribution of relative humidity, *J. Atmos. Sci.*, **34:** 241–259.

Meehl, G.A. (1990), Seasonal cycle forcing of El Niño / Southern Oscillation in a global coupled ocean–atmosphere GCM, *J. Climate*, **3:** 72–98.

Peixoto, J. and A. Oort (1992), *Physics of climate*, AIP Press, 520 pp.

Phillips, N.A. (1973), *Principles of large scale numerical weather prediction, Dynamic Meteorology*, Ed. P. Morel, 1–96 Dordrecht–Holland, D. Reidel Publishing Comp. 1–96.

Posey, J. W., and P. F. Clapp (1964), Global distribution of normal surface albedo, *Geofis. Ins.*, **4:** 33–48.

Schlesinger M.E. and W.L. Gates (1980), The January and July performance of the OSU two–level atmospheric general circulation model, *J. Atmos. Sci.*, **37:** 1914–1943.

Simmonds, I. (1985), Analysis of the "spinning" of a global circulation model, *J. Geoph. Res.*, **90:** 5637–5660.

Tao Shiyan and Chen Longxun (1988), A review of recent research on the East Asian Summer Monsoon in China,

Monsoon Meteorology, Oxford Univ. Press, London, 60–92.

Wang Bin (1995), Interdecadal changes in El Nino onset in the last four decades, *J. Climate*, **8(2):** 267–285.

Wu Guoxiong and Huanzhu Liu (1987), *Time mean global general circulation statistics*, China Meteorological Press, 212 pp. (in Chinese).

Xue Fong (1992), *Statistical analyses of the climate simulation of the IAP GCM and the model characteristics*, Ph.D. Theses, Inst. Atmos. Phy., Chinese Academy of Sciences, 173 pp.

Ye Duzheng and Yuxi Gao (1979), Meteorology of the Tibetan Plateau, Science Press, 278 pp.

Yuan, C. G. (1990), Progress in the research of short–term climate prediction, *Scientia Atmospherica Sinica*, **14:** 250–255 (in Chinese).

Zeng Qingcun (1963), Characteristic parameter and dynamical equation of atmospheric motions, *Acta Meteor. Sinica*, **33:** 472–483 (in Chinese).

Zeng Qingcun (1990), IAP GCM and its application to the climate studies, *Climate Change, Dynamics, and Modelling*, The 3rd International Summer Colloquium of LASG, Ed. Zeng et al., 225–256.

Zeng Q. C., C. G. Yuan, X. H. Zhang, X. Z. Liang and N. Bao (1987), A global gridpoint general circulation model, Collection of papers presented at the WMO / IUGG NWP Symposium, Tokyo, 4–8 August 1986, *Special volumn of J. Meteor. Soc. Japan*, 421–430.

Zeng Q. C., X. H. Zhang, X. Z. Liang, C. G. Yuan and S. F. Chen (1989), *Documentation of IAP Two–Level atmospheric general circulation model*, DOE / ER / 60314–HI, TRO44, 383 pp.

Zhang Xuehong, Bao Ning, Yu Rucong and Wang Wanqiu (1992), Coupling scheme experiments based on an atmospheric and oceanic GCM, Chinese *J. Atmos. Sci.*, **16(2):** 129–144.

Zhang Xuehong, Chen Keming, Jin Xiangzhe, Lin Wuying, Yu Yongqiang (1993), A twenty–layer oceanic general circulation model, *Report at the 1993 Annual Conference of LASG*, Beijing Jan. 10–11, 1994.

Zhang X.H. and X.Z. Liang (1989), Comparison and examination of the dynamic frameworks of IAP and OSU AGCM, *Adv. Atmos. Sci.*, **6:** 265–274.